J|A|C|S ARTICLES

Published on Web 12/08/2010

Synthesis of Nanocrystals with Variable High-Index Pd Facets through the Controlled Heteroepitaxial Growth of Trisoctahedral Au Templates

Yue Yu, Qingbo Zhang, Bo Liu, and Jim Yang Lee*

Department of Chemical and Biomolecular Engineering, National University of Singapore, 10 Kent Ridge Crescent, Singapore 119260, Republic of Singapore

Received August 17, 2010; E-mail: cheleejy@nus.edu.sg

Abstract: The shape-controlled synthesis of noble metal nanocrystals (NCs) bounded by high-index facets is a current research interest because the products have the potential of significantly improving the catalytic performance of NCs in industrially important reactions. This study reports a versatile method for synthesizing polyhedral NCs enclosed by a variety of high-index Pd facets. The method is based on the heteroepitaxial growth of Pd layers on concave trisoctahedral (TOH) gold NC seeds under careful control of the growth kinetics. Polyhedral Au@Pd NCs with three different classes of high-index facets, including concave TOH NCs with {*hhl*} facets, concave hexoctahedral (HOH) NCs with {*hkl*} facets, and tetrahexahedral (THH) NCs with {*hk*0} facets, can be formed in high yield. The Miller indices of NCs are also modifiable, and we have used the THH NCs as a demonstrative example. The catalytic activities of these NCs were evaluated by the structure-sensitive reaction of formic acid electro-oxidation. The results showed that the high-index facets are generally more active than the low-index facets. In summary, a seeded growth process based on concave high-index faceted monometallic TOH NC templates and careful control of the growth kinetics is a simple and effective strategy for the synthesis of noble metal NCs with high-index facets. It also offers tailorability of the surface structure in shape-controlled synthesis.

1. Introduction

High-index surface planes of noble metals denoted by a set of Miller indices {*hkl*} with at least one of the indices greater than unity are often catalytically more active than the close-packed low-index planes of the same metal.[1−4] The reason has been attributed to the presence of a high density of atomic steps and kinks.[2−6] The lure and potential of enhanced catalytic performance has spurred the search for shape-controlled synthesis of noble metal nanocrystals (NCs) with high-index facets.[1,4] The different types of polyhedral NCs and their surface facets could be mapped onto a triangular diagram, as shown in Scheme 1A.[1] At the three vertices are polyhedrons enclosed by three low-index facets: octahedrons with {111} facets, cubes with {100} facets, and rhombic dodecahedrons with {110} facets. The polyhedrons on the sides and within the triangle represent four types of polyhedrons enclosed by high-index facets. Each polyhedron type is associated with a specific class of high-index facets, for example, trisoctahedral (TOH) NCs with {*hhl*} facets and tetrahexahedral (THH) NCs with {*hk*0} facets. Moving along the side of the triangle or anywhere within the triangle, the geometrical parameters of the polyhedral type change, along with changes in the Miller indices of the high-index facets, but the class is conserved. Hence, polyhedral NCs can, in principle, provide a large variety of high-index facets through variations in their classes and the Miller indices within each class.[1] In practice, however, noble metal NCs with high-index facets have only been synthesized in a limited number of shapes and Miller indices, e.g., THH Pt[2] and Pd[7] NCs with high-index {730} facets by electrochemical deposition methods and elongated THH Au NCs with exposed {730} facets,[8] THH Au NCs with {520} facets,[9] and TOH Au NCs with {221} or {331} facets[10,11] by solution chemistry methods. The synthesis of NCs enclosed by high-index facets other than the above remains a challenge because of the high energy and fast growth rate of the high-index facets.[12,13]

In this study, we have successfully synthesized polyhedral NCs enclosed by modifiable high-index Pd facets where both the class of the high-index facets and the Miller indices within the class could be changed. The synthesis is based on the

(1) Tian, N.; Zhou, Z. Y.; Sun, S. G. *J. Phys. Chem. C* **2008**, *112*, 19801–19817.
(2) Tian, N.; Zhou, Z. Y.; Sun, S. G.; Ding, Y.; Wang, Z. L. *Science* **2007**, *316*, 732–735.
(3) Zhou, Z. Y.; Huang, Z. Z.; Chen, D. J.; Wang, Q.; Tian, N.; Sun, S. G. *Angew. Chem., Int. Ed.* **2010**, *49*, 411–414.
(4) Xiong, Y. J.; Wiley, B.; Xia, Y. N. *Angew. Chem., Int. Ed.* **2007**, *46*, 7157–7159.
(5) Sun, S. G.; Chen, A. C.; Huang, T. S.; Li, J. B.; Tian, Z. W. *J. Electroanal. Chem.* **1992**, *340*, 213–226.
(6) Somorjai, G. A.; Blakely, D. W. *Nature* **1975**, *258*, 580–583.
(7) Tian, N.; Zhou, Z. Y.; Yu, N. F.; Wang, L. Y.; Sun, S. G. *J. Am. Chem. Soc.* **2010**, *132*, 7580–7581.
(8) Ming, T.; Feng, W.; Tang, Q.; Wang, F.; Sun, L. D.; Wang, J. F.; Yan, C. H. *J. Am. Chem. Soc.* **2009**, *131*, 16350–16351.
(9) Li, J.; Wang, L. H.; Liu, L.; Guo, L.; Han, X. D.; Zhang, Z. *Chem. Commun.* **2010**, *46*, 5109–5111.
(10) Ma, Y. Y.; Kuang, Q.; Jiang, Z. Y.; Xie, Z. X.; Huang, R. B.; Zheng, L. S. *Angew. Chem., Int. Ed.* **2008**, *47*, 8901–8904.
(11) Yu, Y.; Zhang, Q. B.; Lu, X. M.; Lee, J. Y. *J. Phys. Chem. C* **2010**, *114*, 11119–11126.
(12) Xia, Y.; Xiong, Y.; Lim, B.; Skrabalak, S. E. *Angew. Chem., Int. Ed.* **2009**, *48*, 60–103.
(13) Tao, A. R.; Habas, S.; Yang, P. D. *Small* **2008**, *4*, 310–325.

10.1021/ja107405x

Scheme 1. (A) Triangular Diagram Showing fcc Metal Polyhedrons Bounded by Different Crystallographic Facets and (B) Schematic Illustration of the Reaction Regions That Form Au@Pd NCs with Different Polyhedral Shapes and Different High-Index Facets[a]

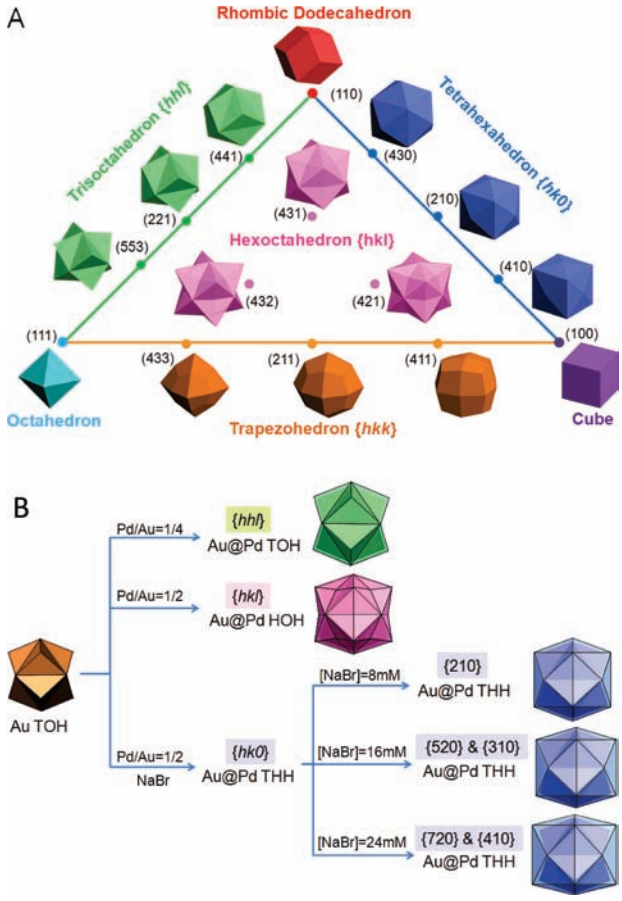

[a] All geometrical models are oriented in the ⟨110⟩ direction.

heteroepitaxial growth of Pd layers on concave TOH gold NC seeds under carefully controlled growth conditions. The use of the TOH Au NC as the template, which itself is a concave polyhedron with high-index facets, is critical. Consequently, polyhedral Au@Pd NCs enclosed by three different classes of high-index facets, including concave TOH NCs with {*hhl*} facets, concave hexoctahedral (HOH) NCs with {*hkl*} facets, and THH NCs with {*hk*0} facets, could be formed in high yield by varying the Pd/Au atomic ratio and by NaBr addition, as shown in Scheme 1B. The Miller indices within each polyhedral type could also be varied by controlling the growth kinetics; we will use the THH NCs and NaBr concentration adjustments as an example. The electro-oxidation of formic acid was used to evaluate the electrocatalytic properties of the Au@Pd NCs.

2. Experimental Section

2.1. Materials. Hydrogen tetrachloroaurate(III) hydrate ($HAuCl_4 \cdot xH_2O$, Alfa Aesar, 49.87% Au), palladium(II) chloride ($PdCl_2$, Sigma Aldrich, 98%), sodium borohydride ($NaBH_4$, Fluka, 98%), cetyltrimethylammonium chloride (CTAC, Alfa Aesar, 95+%), cetyltrimethylammonium bromide (CTAB, Sigma Aldrich, ≥98%), and L-ascorbic acid (Merck, 99%) were used as received. Ultrapure Millipore water (18.2 MΩ) was used as the solvent throughout. All glassware was cleaned in Aqua Regia and rinsed with ethanol and ultrapure water. A 10 mM H_2PdCl_4 solution was prepared by dissolving 44.5 mg of $PdCl_2$ in 25 mL of 20 mM HCl solution.

2.2. Preparation of Gold TOH Seeds. The synthesis of Au TOH NCs was based on a growth process using the octahedral Au NC seeds, and hence the latter were prepared first. In a typical synthesis, 7 mL of 75 mM CTAB solution was first prepared by heating at 30 °C with stirring to dissolve the CTAB. Next, 87.5 μL of 20 mM $HAuCl_4$ solution was added to the CTAB solution, and then 0.6 mL of an ice-cold $NaBH_4$ solution (10 mM) was injected quickly into the mixture under vigorous mixing to form a brown seed solution. Stirring continued gently at 30 °C for 2−5 h to decompose the excess $NaBH_4$. The seed solution was then diluted 100-fold with ultrapure water. A growth solution was prepared by adding 25 μL of 20 mM $HAuCl_4$ solution and 0.387 mL of 38.8 mM ascorbic acid (in that order) into 12.1 mL of 16.5 mM CTAB solution in a clean test tube at 28 °C with thorough mixing after each addition. Finally, 0.15 mL of the diluted seed solution was added to the growth solution and thoroughly mixed. The mixture was left unperturbed at 28 °C overnight. The color of the solution changed to pink, indicating the formation of gold NCs.

The growth solution for the synthesis of TOH gold NCs was prepared by adding 0.125 mL of 20 mM $HAuCl_4$ solution and 3.06 mL of 38.8 mM ascorbic acid solution to 9 mL of 22 mM CTAC solution. Next, 6.5 mL of the octahedral seed solution was added to this growth solution and thoroughly mixed. The mixture was left unperturbed overnight. For the growth of TOH NCs into larger TOH particles, 4 mL of the as-prepared TOH NC solution was added to 9 mL of 22 mM CTAC solution and mixed, and then 3.06 mL of 38.8 mM ascorbic acid solution was introduced, followed by the addition of 0.125 mL of 20 mM $HAuCl_4$. The solution was thoroughly mixed after each addition and left overnight.

2.3. Synthesis of TOH, HOH, and THH Au@Pd NCs. The heteroepitaxial growth of Pd on Au TOH NCs was accomplished by introducing H_2PdCl_4 and ascorbic acid into the Au TOH NC solution. For the synthesis of TOH Au@Pd NCs, 0.258 mL of 38.8 mM ascorbic acid and 24 μL of 10 mM H_2PdCl_4 were added to 5 mL of Au TOH NC solution for a Pd/Au atomic ratio of 1/4. For the synthesis of Au@Pd HOH NCs, 0.258 mL of 38.8 mM ascorbic acid and 48 μL of 10 mM H_2PdCl_4 were added to 5 mL of Au TOH NC solution (Pd/Au atomic ratio was 1/2). The THH Au@Pd NCs were prepared similarly to the HOH Au@Pd NCs but with different amounts of 0.5 M NaBr added to the growth solution. The mixture was shaken well and left overnight. The resultant Au@Pd NC solutions were centrifuged at 8000 rpm for 3 min. The precipitates were redispersed in deionized water and centrifuged two more times (6000 rpm, 3 min) to remove the excess reactants.

2.4. Materials Characterizations. The structure and composition of the NCs were analyzed by transmission electron microscopy (TEM), high-resolution TEM (HRTEM), and energy-dispersive X-ray spectroscopy (EDX) on JEM-2010 and JEM-2100F (JEOL) microscopes operating at the 200 kV accelerating voltage. Field emission scanning electron microscopy (FESEM) (JEOL JSM-6700F, equipped with scanning TEM (STEM) function operating at 25 kV) was used to examine the general product morphology. EM samples were prepared by dispensing a drop of the washed product on a copper grid, followed by drying in air at room temperature.

2.5. Electrochemical Measurements. A glassy carbon electrode (diameter 5 mm) was carefully polished and washed before each experiment. A washed Au@Pd NC suspension was dispensed onto the surface of the glassy carbon electrode to a gold mass loading of 40 μg and dried at 35 °C. The deposited NC layer was then coated with a 10 μL Nafion solution, prepared by diluting 50 μL of commercial 5 wt % Nafion solution with 5 mL of ethanol and 5 mL of ultrapure water.

Electrochemical measurements were carried out in a conventional three-electrode glass cell under the control of an Autolab PGSTAT12 potentiostat/galvanostat. A Pt gauze and a Ag|AgCl (3 M KCl) electrode were used as the counter electrode and the reference electrode, respectively. The supporting electrolyte was

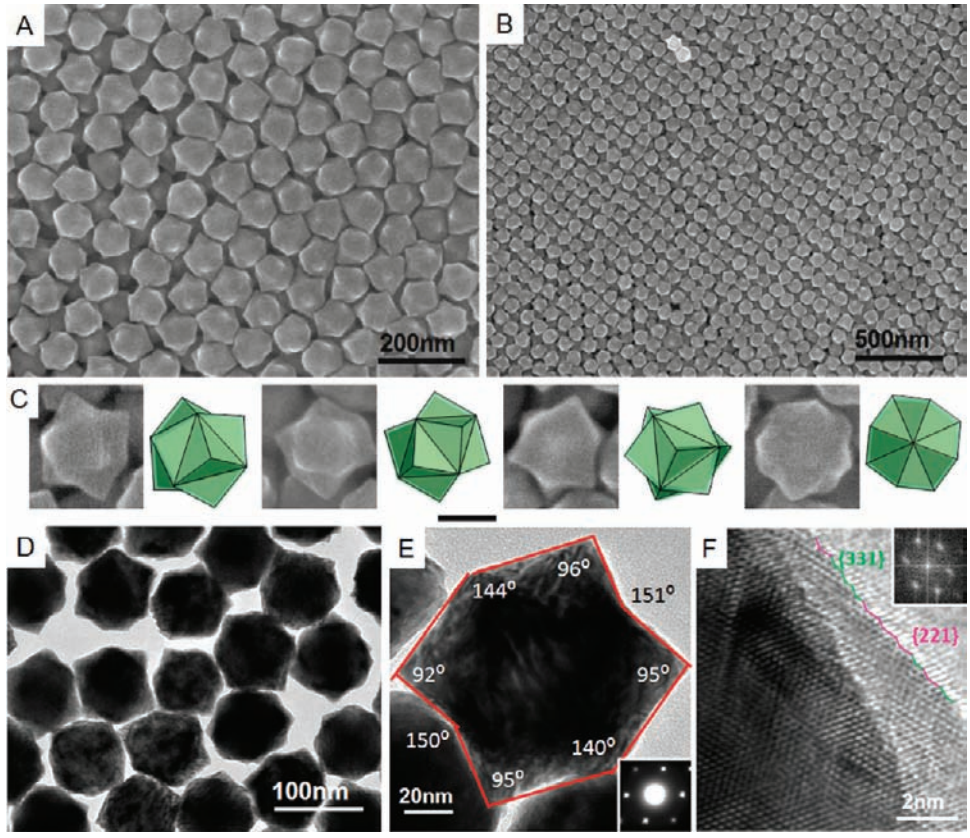

Figure 1. SEM images of TOH Au@Pd NCs at (A) high and (B) low magnifications. (C) Individual NCs in different orientations, with the corresponding geometrical models shown on the right of each SEM image. The scale bar is 50 nm. (D) TEM image of overall morphology of TOH Au@Pd NCs. (E) TEM image of a single TOH Au@Pd NCs viewed from the ⟨110⟩ direction and the corresponding electron diffraction pattern (inset). The measured projection angles are marked. (F) HRTEM image of an edge-on facet of TOH Au@Pd NC, showing that the atomic steps in the surface are made of {221} and {331} subfacets. Inset is the corresponding FFT pattern.

0.1 M $HClO_4$ aqueous solution with or without 1 M formic acid. The solution was deaerated with argon before each experiment. Electrochemical measurements were based on cyclic voltammetry carried out at a scan rate of 20 mV/s for electrochemically active surface area measurements; and at a scan rate of 10 mV/s for formic acid oxidation. The currents in formic acid oxidation were normalized by the surface areas estimated from the hydrogen adsorption/desorption cyclic voltammograms in perchloric acid solution.[7]

3. Results and Discussion

3.1. Synthesis of Polyhedral NCs with High-Index Facets of Variable Classes. In a typical synthesis, concave TOH Au NCs (Figure S1, Supporting Information), which were prepared with a slight modification of our previous method,[11] were used as the templating seeds. Au@Pd NCs could then be prepared by the heteroepitaxial growth of a Pd layer from the ascorbic acid reduction of H_2PdCl_4 in the presence of the seeds. Concave TOH Au NCs were selected as the template because their concave shape and protruded corners offer a versatile geometry for tailoring a variety of high-index facets. The successful growth of a Pd layer on the Au seeds was confirmed by mapping the Au and Pd elements of the NCs (Figure S2−S4, Supporting Information).

Polyhedral NCs enclosed by various classes of high-index facets could be formed in high yield by adjusting the Pd/Au atomic ratio and NaBr addition, as shown in Scheme 1B. When the Pd/Au atomic ratio was 1/4, the growth of the Pd layer followed the contour of the underlying concave TOH Au templates. The conformal growth led to a majority of the resultant NCs adopting the concave TOH shape, as shown in the SEM images of Figure 1A,B. A TOH is an octahedron with each of its facets capped by a triangular pyramid.[10,11] It is therefore a polyhedron bounded by 24 high-index {*hhl*} ($h > l > 0$) facets.[1,10,11] The good agreement between the SEM images of the NCs and the geometrical models (shown on the right of each image) confirms the TOH geometry of the NCs (Figure 1C). The formation of Au@Pd core−shell structure was also implicated by the alternating bright and dark fringes in the TEM image (Figure 1D) which came from the superposition of two misfit crystalline lattices in a Au@Pd core−shell construction.[14,15] For NCs enclosed by high-index facets, the Miller indices of high-index facets could be determined from the projection angles in selected crystallographic directions.[1,2] The projection angles corresponding to ideal polyhedral crystals enclosed by high-index facets with different Miller indices are given in Table S1 (Supporting Information). Figure 1E shows the TEM image of an individual TOH NC viewed from the ⟨110⟩ direction, as confirmed by the electron diffraction pattern (inset of Figure 1E). In this orientation, four facets can be projected edge-on.[1,11] The four edge-on facets were identified to be the {552} facets by comparing the measured projection angles with the calculated ones. The Miller indices of high-index facets could also be determined from the arrangement of the atoms in the edge-on

(14) Lee, Y. W.; Kim, M.; Kim, Z. H.; Han, S. W. *J. Am. Chem. Soc.* **2009**, *131*, 17036–17037.
(15) Fan, F. R.; Liu, D. Y.; Wu, Y. F.; Duan, S.; Xie, Z. X.; Jiang, Z. Y.; Tian, Z. Q. *J. Am. Chem. Soc.* **2008**, *130*, 6949–6951.

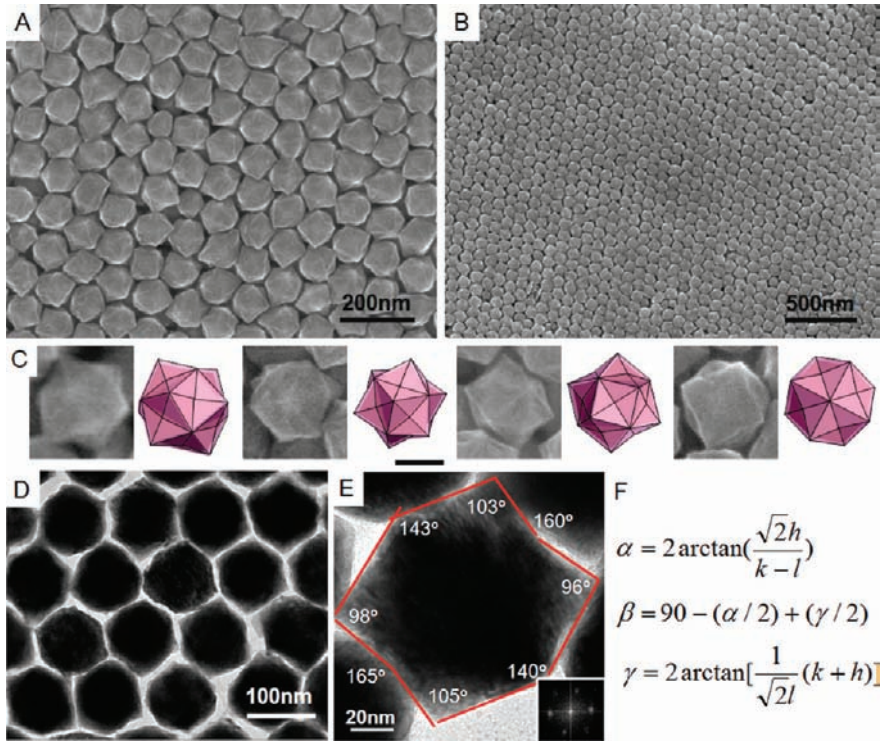

Figure 2. SEM images of HOH Au@Pd NCs in (A) high and (B) low magnifications. (C) Individual HOH NCs in different orientations with the corresponding geometrical models shown on the right of each SEM image. The scale bar is 50 nm. (D) TEM image of overall morphology of HOH Au@Pd NCs. (E) TEM image of a single HOH Au@Pd NCs viewed from the ⟨110⟩ direction and the corresponding FFT pattern (inset). The measured projection angles are marked. (F) Relations between the projection angles and Miller indices of HOH NC in the ⟨110⟩ direction based on the HOH geometry.

facets.[1,2,16] A step notation can be used to describe the high-index planes as $m(h_tk_tl_t)\times(h_sk_sl_s)$, which means m atomic width of $(h_tk_tl_t)$ terraces separated by monatomic $(h_sk_sl_s)$ steps.[16] The edge-on facet of the TOH Au@Pd NC shown in Figure 1F shows a series of alternating {221} (3(111)×(110), magenta color) and {331} (2(111)×(110), green color) subfacets, resulting in an overall profile which is close to the {552} facets. The atomic models of {221}, {552}, and {331} planes with (111) terraces and (110) steps are shown in Figure S5 (Supporting Information). The HRTEM image in Figure 1F also shows no disruption of the lattice pattern at the Au/Pd interfaces, indicating that the Pd layer was formed through the heteroepitaxial growth of Pd on the Au seed.

When the Pd/Au atomic ratio was increased to 1/2, the shape of the Au@Pd NCs transformed from concave TOH to concave HOH, which can be seen in the SEM images of Figure 2A,B. A HOH can be visualized as a TOH with its ⟨111⟩ edges bending outward from the edge centers.[1] As a result, each $\{h'h'l'\}$ facet is split into two $\{hkl\}$ facets. It is therefore a polyhedron bounded by 48 high-index $\{hkl\}$ $(h > k > l > 0)$ facets. It can also be seen as a THH with its ⟨100⟩ edges contracting inward from the edge centers, splitting each $\{h'k'0\}$ facet into two $\{hkl\}$ facets. The HOH geometry was confirmed by the good agreement between the SEM images of the NCs and the geometrical models of concave HOH in the same orientation (Figure 2C). The fringes overlaying the NCs in the TEM image of Figure 2D signify the successful overgrowth of a Pd shell on the Au templates. The relations between the Miller indices $\{hkl\}$ and the projection angles of an ideal HOH NC viewed from the ⟨110⟩ direction are described by the set of equations in Figure 2F, which were derived from the geometry. It is worth noting that these equations are also applicable to TOH ($h = k$), THH ($l = 0$), and trapezohedral NCs ($k = l$). The projection angles of the NC measured from Figure 2E agrees well with the theoretical values of {432} facets. The {432} facet can be expressed in terms of the step notation as 2(111)×(210).[16] Since the step itself is a high-index (210) subfacet, the Miller indices of the HOH NCs could not be derived from the atomic arrangement in the edge-on facets.

In addition to high-index faceted TOH and HOH Au@Pd NCs, THH Au@Pd NCs could also be obtained by adding NaBr to the growth solution with a Pd/Au atomic ratio of 1/2 which was used for the HOH NCs. Figure 3A,B shows the SEM images in high and low magnifications of the THH NCs obtained with 16 mM NaBr concentration in the growth solution. A THH can be seen as a cube with each facet capped by a square pyramid.[1,2,7−9] It is bounded by 24 high-index $\{hk0\}$ $(h > k > 0)$ facets. The SEM images of the NCs are consistent with the geometrical model of THH in different orientations (Figure 3C). The formation of a Pd layer on the Au core could also be confirmed from the fringes overlaying the NCs (Figure 3D). When the imaging electron beam is parallel to the ⟨100⟩ direction, the NC will be projected as an octagon. The eight sides of the octagon are the facets of the THH NCs that are imaged edge-on. A comparison of the measured and calculated projection angles shows that the edge-on facets of the THH NC in Figure 3E consisted of both {310} and {520} facets. The edge-on facet of the THH NC in Figure 3F was parallel to the {520} facet consisting of alternating {310} (3(100)×(110), blue color) and {210} (2(100)×(110), red color) subfacets.

The comparison of the SEM images of TOH, HOH, and THH NCs viewed from the ⟨111⟩, ⟨110⟩, and ⟨100⟩ directions and TEM images viewed from the ⟨110⟩ directions are given in

(16) Vanhove, M. A.; Somorjai, G. A. *Surf. Sci.* **1980**, *92*, 489–518.

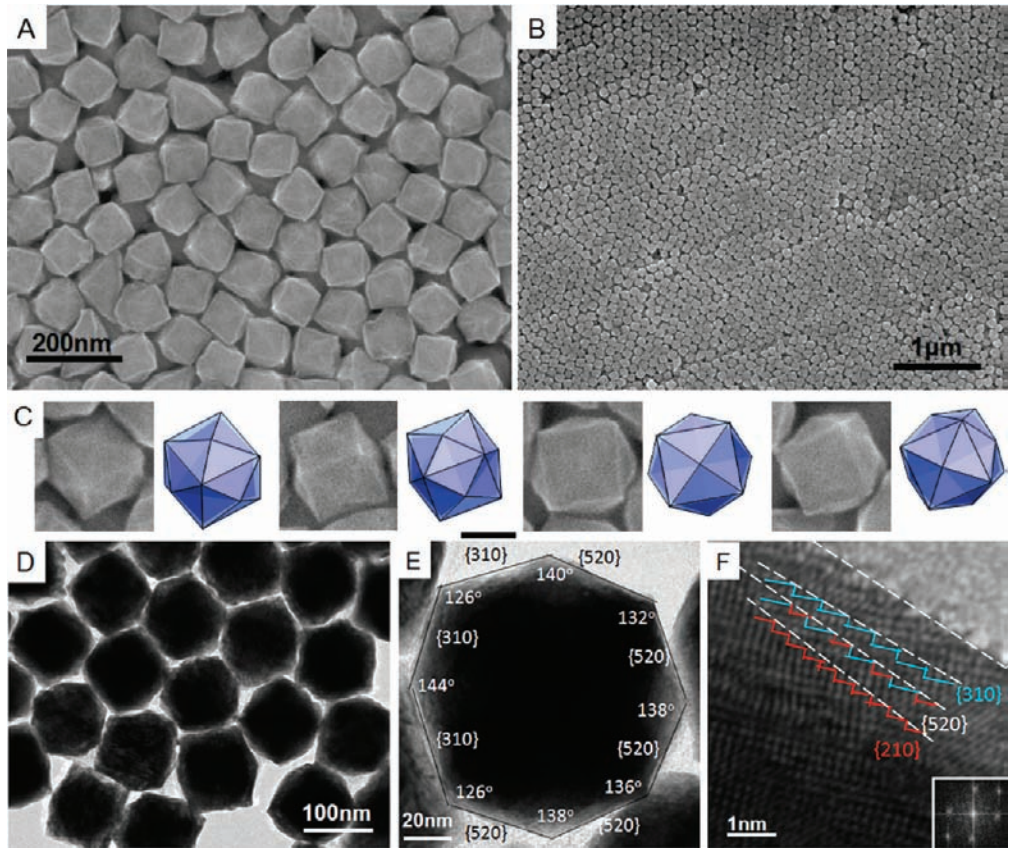

Figure 3. SEM images showing the overall morphology of THH Au@Pd NCs in (A) high and (B) low magnifications and (C) individual THH NCs in different orientations, with the corresponding geometrical models shown on the right of each SEM image. The scale bar is 50 nm. (D) TEM image showing the overall morphology of THH Au@Pd NCs. (E) TEM image of a single THH Au@Pd NC viewed from the ⟨100⟩ direction. The measured projection angles are marked. The projection angles indicate that the exposed surface is made up of {310} and {520} facets. (F) HRTEM image of an edge-on facet of THH Au@Pd NC, showing the parallelism between the surface facet and the {520} plane. Inset is the corresponding FFT pattern.

Figures S6 and S7 (Supporting Information) to help in visualizing the difference between these three types of polyhedral NCs.

3.2. Synthesis of Polyhedral NCs with High-Index Facets of Variable Miller Indices. The seeded heteroepitaxial growth on concave TOH Au NCs is a versatile technique to synthesize NCs with different classes of high-index facets, and hence different polyhedral shapes. In addition, the Miller indices of the high-index facets in each class could also be altered by manipulating the growth kinetics. The variations of Miller indices can be deduced from the changes in the geometrical parameters of the polyhedron, while the overall polyhedral type is preserved (Scheme 1A). The following discussion is based on the THH NCs, which are used as an illustrative example.

The concentration of Br^- provided the means for kinetic control. NaBr was added to the growth solution to final concentrations of 8, 16, and 24 mM, while keeping the Pd/Au atomic ratio at 1/2. The SEM images in Figures 4A, 3A, and 4B show that the NCs obtained under these conditions were all THH polyhedrons. A closer examination of the SEM images, however, revealed some slight differences in the THH geometries, which depended on the NaBr concentration. The height of the square pyramids on the cubic base was taller for THH NCs synthesized with 8 mM NaBr in the growth solution, and 24 mM NaBr produced THH NCs with flatter square pyramids. The geometrical difference was also visible in the TEM images. Figure 4C−E shows TEM images of THH NCs viewed from the ⟨110⟩ direction, prepared at different NaBr concentrations. The Miller indices {*hk*0} of the exposed facets of the THH NCs are related to their geometrical parameters, i.e., the height of

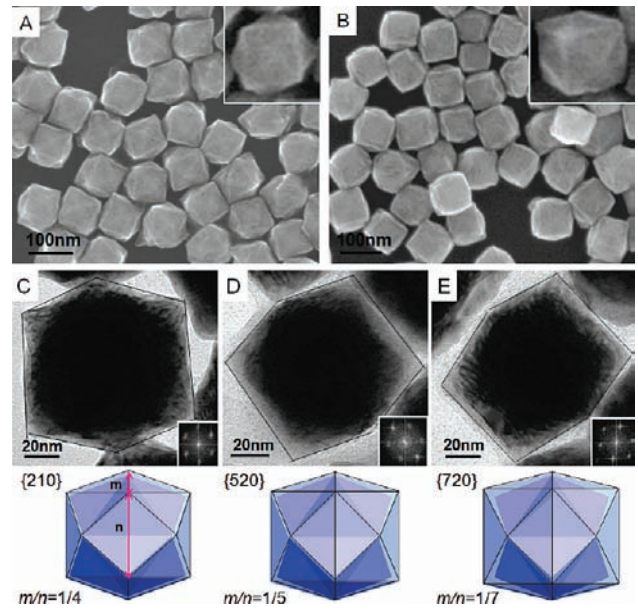

Figure 4. SEM images of THH Au@Pd NCs prepared with NaBr concentrations of (A) 8 and (B) 24 mM in the growth solution. Representative TEM images of THH Au@Pd NCs obtained with NaBr concentrations of (C) 8, (D) 16, and (E) 24 mM viewed from the ⟨110⟩ direction. Below each TEM image is the respective geometrical model of THH NCs enclosed by {210}, {520}, and {720} facets. *m* and *n* are geometrical parameters for the THH NCs corresponding to the height of the square pyramids on the cubic base and the edge length of the cubic base, respectively, with the relation $m/n = k/2h$.

Scheme 2. (A) Schematic Illustration of Growth from TOH to HOH or THH NCs[a] and (B) Schematic Illustration of the Cross Section of the NCs Viewed from the ⟨110⟩ Directions, Showing the Transformations between Different Polyhedral NCs[b]

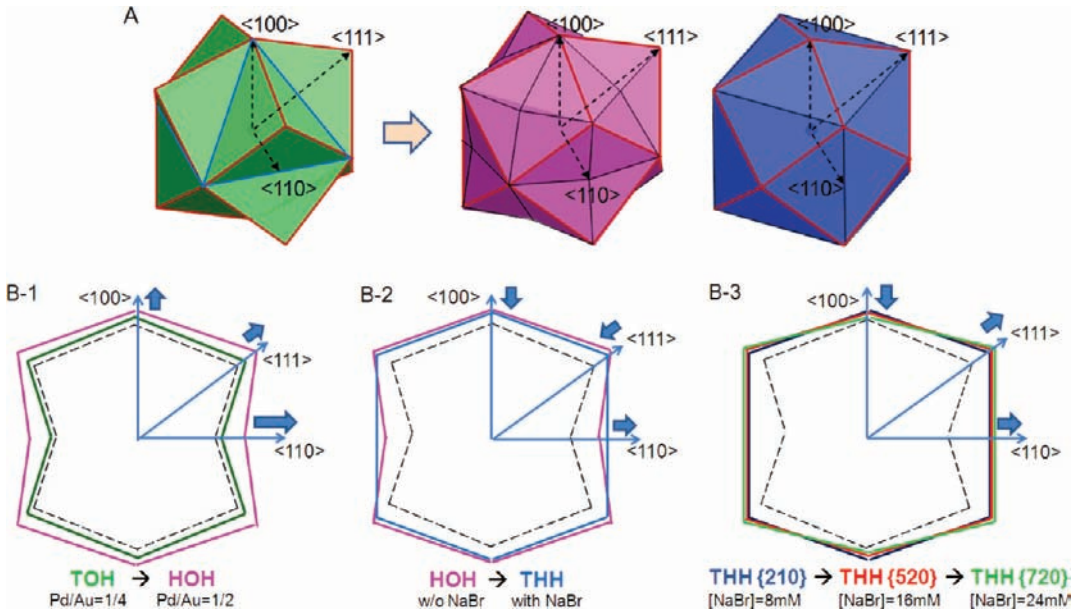

[a] The ⟨111⟩, ⟨100⟩, and ⟨110⟩ directions are marked. The red edges of the TOH NCs are the "convex edges", and the blue ones are the "concave edges". Growth from TOH to HOH or THH involves the filling of the concave space and the restraining effect of the "convex edges" (growth in the ⟨110⟩ directions). [b] (B-1) Shape transformation from TOH to HOH with increase in the Pd amount. The ⟨110⟩ direction grows faster relative to the ⟨100⟩ and ⟨111⟩ directions. (B-2) Shape transformation from HOH to THH with the addition of NaBr. Here the relative growth rate in the ⟨110⟩ direction increases while the rates in the ⟨100⟩ and ⟨111⟩ directions decrease. (B-3) Shape transformation of THH with increase in the *h*/*k* value of {*hk*0} facets caused by the increase in NaBr concentration. Here the growth rate along the ⟨100⟩ direction decreases while the rates along the ⟨111⟩ and ⟨110⟩ directions increase.

the square pyramid (*m*) and the edge length of the cubic base (*n*), by the equation $h/k = n/2m$. The *m*/*n* values of the THH NCs shown in Figure 4C−E were 1/4.07, 1/5.11, and 1/7.09 respectively, suggesting that the Miller indices of THH NCs prepared with different NaBr concentrations were different. The variability of the Miller indices could also be detected by measuring the projection angles of the THH NCs viewed from the ⟨100⟩ directions. The projection angle analysis allowed the Miller indices of the THH NCs to be determined quantitatively (Figure S8A−C, Supporting Information). By comparing the measured projection angles with the calculated values, the majority of the THH NCs synthesized at a NaBr concentration of 8 mM were found to be enclosed by {210} facets. With 16 mM NaBr, the THH NCs were enclosed by {310} and {520} facets, and with 24 mM NaBr, the NCs were enclosed by {720} and {410} facets. The Miller indices of the exposed facets were further confirmed by examining the atomic arrangement in the edge-on facets in HRTEM images. {210} and {720} facets, consisting of (100) terraces separated by (110) steps, were found in the HRTEM images in Figure S8D,E. All of the above analyses indicate that the Miller indices of the exposed {*hk*0} facets of THH NCs are modifiable, with the *h*/*k* value increasing with the increase in NaBr concentration. The atomic models of {*hk*0} planes with various *h*/*k* values are given in Figure S8F. With the increase in the *h*/*k* value, the atomic width of the (100) terraces of the {*hk*0} planes increases.

As a final illustration of the adjustability of the Miller indices, THH NCs with a more significantly different appearance were prepared by the further growth of THH NCs synthesized at a NaBr concentration of 24 mM. As shown in Figure S9 (Supporting Information), the resultant NCs were cube-like THHs which are distinguishably different from the THH NCs shown in Figures 3 and 4. In this case the square pyramids on the cubic base were almost flat, and the facets were approximately {100} planes. These are indications that the Miller indices can be varied over a wide range of values.

3.3. Mechanisms. The shape of the Au@Pd NCs produced by the seeded growth process is determined by the templating effect of the concave TOH Au seeds and the growth kinetics of the Pd atoms. Under the slow reduction rate due to the use of a mild reducing agent such as ascorbic acid, Pd atoms would prefer to grow in a layer-by-layer manner to form a Pd shell on the Au NC seeds.[15,17,18] When the amount of Pd was low (Pd/Au = 1/4), the Pd shell followed the shape of the underlying seed. The templating effect of the Au seeds dominated in this case to result in TOH Au@Pd NCs. With more Pd atoms deposited on the NC surface (Pd/Au = 1/2), the growth kinetics of Pd began to exert its influence on shape evolution. It has been demonstrated that the polyhedral shape of NCs is determined by the differences in the relative growth rates of three low-index facets.[11−13,19,20] Usually, Pd {110} facets with their high surface energy would grow faster than the Pd {111} and {100} facets.[17] The ⟨111⟩, ⟨100⟩, and ⟨110⟩ directions in TOH, HOH, and THH NCs are labeled in Scheme 2A. For a TOH NC, the ⟨110⟩ direction is directed from the center of the NC to the centers of the "concave edges" (the edges between two concave facets, shown in blue). The faster growth rate in the ⟨110⟩ directions would gradually fill the concave space of the TOH NC. On the other hand, the ⟨100⟩ and ⟨111⟩ directions are directed from the center of the NC to the two ends of the

(17) Xiang, Y. J.; Wu, X. C.; Liu, D. F.; Jiang, X. Y.; Chu, W. G.; Li, Z. Y.; Ma, Y.; Zhou, W. Y.; Xie, S. S. *Nano Lett.* **2006**, *6*, 2290–2294.
(18) Lim, B.; Kobayashi, H.; Yu, T.; Wang, J. G.; Kim, M. J.; Li, Z. Y.; Rycenga, M.; Xia, Y. *J. Am. Chem. Soc.* **2010**, *132*, 2506–2507.
(19) Wang, Z. L. *J. Phys. Chem. B* **2000**, *104*, 1153–1175.
(20) Grzelczak, M.; Perez-Juste, J.; Mulvaney, P.; Liz-Marzan, L. M. *Chem. Soc. Rev.* **2008**, *37*, 1783–1791.

"convex edges" (the edges between two convex facets, shown in red). As a result of the slower growth rates in the ⟨111⟩ and ⟨100⟩ directions, the shape of the NC would be "restrained" by the "convex edges" of the TOH seed. As shown in Scheme 2A and Figure S7 (Supporting Information), the filling of the concave space and the restraining effect of the "convex edges" would aid the shape transformation from TOH to HOH or THH.

The formation of HOH or THH NCs is dependent on the growth rate in the ⟨110⟩ direction relative to the growth rates in the ⟨100⟩ and ⟨111⟩ directions (Scheme 2B and Figure S7). Geometrically, THH is favored by a high growth rate in the ⟨110⟩ direction. If the growth rate in the ⟨110⟩ direction is not as high, the concave space of the TOH is not completely filled and a concave HOH is formed, as shown in Scheme 2B-1,2. The growth kinetics of Pd may be moderated by introducing the Br^- ions. The mixing of NaBr with H_2PdCl_4 replaces the Cl ligand with Br ligand to form $[PdCl_{4-n}Br_n]^{2-}$ ($0 < n \leq 4$). The standard electrode reduction potentials of $[PdCl_4]^{2-}$/Pd and $[PdBr_4]^{2-}$/Pd are 0.59 and 0.49 V, respectively.[21] Therefore, the formation of $[PdCl_{4-n}Br_n]^{2-}$ reduces the thermodynamic driving force for Pd reduction, and the reduction rate is expected to decrease accordingly.[22] A slow reduction rate increases the probability for the Pd atoms to seek the most favorable growth directions (the ⟨110⟩ directions in this case). The difference between the growth rates in the ⟨110⟩ directions and those in the ⟨100⟩ and ⟨111⟩ directions is then emphasized. The increase in the growth rate in the ⟨110⟩ directions in the presence of NaBr therefore transforms TOH into THH rather than HOH.

The Miller indices of THH NCs could also be varied by manipulating the growth kinetics. For THH NCs, the edge length of the cubic base (n) is determined by the growth rates in the ⟨111⟩ and ⟨110⟩ directions, while the height of the square pyramids on the cubic base (m) is determined mainly by the growth rate of the {100} facets relative to the other two low-index facets, as shown in Scheme 2A. The concentration of Br^- ions again provides the means for kinetic control. Br^- ions would preferentially adsorb on the Pd {100} facets,[17,22,23] decreasing the growth rate in the ⟨100⟩ direction and increasing the growth rates in the ⟨111⟩ and ⟨110⟩ directions. Therefore, with the increase in NaBr concentration, the growth rate in the ⟨100⟩ direction is slower. As a result, the height of the square pyramids would decrease relative to the edge length of the cubic base; i.e., the m/n value of the THH NCs decreases (Scheme 2B-3). Consequently, THH NCs enclosed by {hk0} facets with higher h/k values, i.e., a longer atomic width of the (100) terraces, would be formed. When more Pd atoms are available for growth, they would also follow such growth kinetics, with Pd atoms preferentially deposited in the ⟨111⟩ and ⟨110⟩ directions, rendering the growth in the ⟨100⟩ direction the slowest. As a result, THH NCs which are nearly cubic in shape are formed with facets closer to the {100} facets.

3.4. Electrochemical Measurements. The successful synthesis of Au@Pd NCs enclosed with different high-index Pd facets allowed the study of surface-dependent catalytic properties. The electro-oxidation of formic acid was chosen as a probe reaction in this study since its catalysis by Pd is known to be structure sensitive.[24−26] For comparative purposes, cubic and octahedral Au@Pd NCs enclosed by low-index {100} and {111} facets were also prepared by the heteroepitaxial growth of Pd layer on cubic and octahedral Au seeds (Figures S11 and S12, Supporting Information). Figure 5 shows the cyclic voltammograms of formic acid oxidation in 1 M formic acid + 0.1 M $HClO_4$, catalyzed by Au@Pd NCs with different polyhedral shapes enclosed by different crystallographic facets. The peak potentials, peak current densities, and current densities at 0 V (all potentials are referenced to the Ag|AgCl (3 M KCl) standard) of the forward anodic scan from these NCs are summarized in Table S2 and Figure S15 (Supporting Information). The maximum current density of formic acid oxidation in the forward anodic scan followed the order of octahedra < TOH < HOH < cubes = THH. THH NCs enclosed by {hk0} facets and cubic NCs enclosed by {100} facets exhibited the highest oxidation rate of formic acid among the NCs examined in this study. The anodic peak potential depended on the surface structure in the following order: 0.21 V for octahedral NCs, 0.29 V for TOH NCs, 0.31 V for HOH NCs, from 0.32 to 0.41 V for THH NCs with increasing peak potential with the h/k value, and 0.47 V for cubic NCs. The variations in the anodic peak potential among the THH NCs are further evidence that the Miller indices of the THH NCs were different. From the

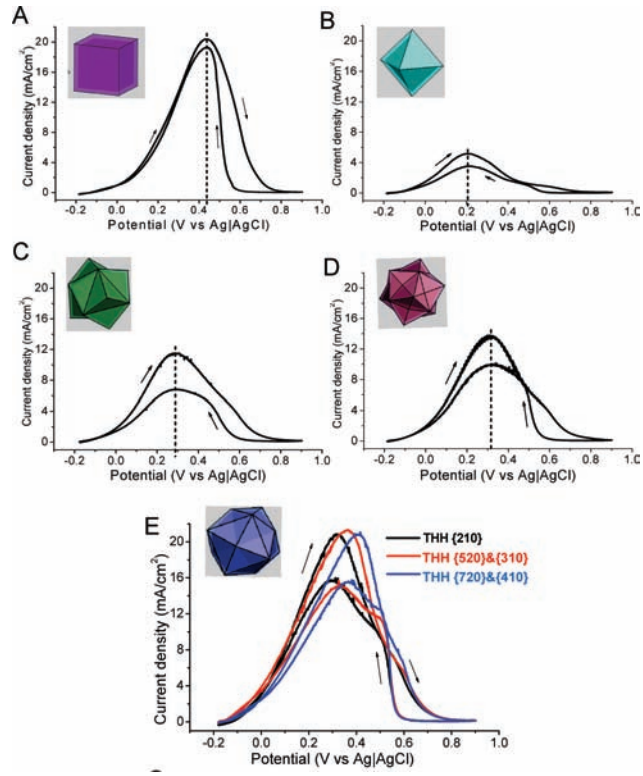

Figure 5. Cyclic voltammograms of formic acid electro-oxidation in 0.1 M $HClO_4$ + 1 M HCOOH on Au@Pd NCs with different polyhedral shapes enclosed by different crystallographic facets. (A) Cubic Au@Pd NCs with {100} facets. (B) Octahedral Au@Pd NCs with {111} facets. (C) TOH Au@Pd NCs with {552} facets. (D) HOH Au@Pd NCs with {432} facets. (E) THH Au@Pd NCs with {hk0} facets of different Miller indices. Scan rate: 10 mV/s.

(21) Chakravorti, M. C.; Subrahmanyam, G. V. B. *Polyhedron* **1992**, *11*, 3191–3195.
(22) Xiong, Y. J.; Cai, H. G.; Yin, Y. D.; Xia, Y. N. *Chem. Phys. Lett.* **2007**, *440*, 273–278.
(23) Xiong, Y. J.; Cai, H. G.; Wiley, B. J.; Wang, J. G.; Kim, M. J.; Xia, Y. N. *J. Am. Chem. Soc.* **2007**, *129*, 3665–3675.
(24) Hoshi, N.; Kida, K.; Nakamura, M.; Nakada, M.; Osada, K. *J. Phys. Chem. B* **2006**, *110*, 12480–12484.
(25) Hoshi, N.; Nakamura, M.; Kida, K. *Electrochem. Commun.* **2007**, *9*, 279–282.
(26) Habas, S. E.; Lee, H.; Radmilovic, V.; Somorjai, G. A.; Yang, P. *Nat. Mater.* **2007**, *6*, 692–697.

viewpoint of practical applications in fuel cells, where a high current density at low potentials is preferable, the current densities at 0 V were also compared.[25] A different activity order was obtained: cubes < octahedra < TOH < HOH < $THH_{\{720\}}$ < $THH_{\{210\}}$ < $THH_{\{520\}}$. In this case, Au@Pd NCs with high-index facets were more active for formic acid oxidation at low potentials than those with low-index facets.

4. Conclusion

Through a controlled heteroepitaxial growth process on preformed Au TOH NC templates, Au@Pd NCs with different polyhedral shapes enclosed by different high-index facets were synthesized. They include concave TOH Au@Pd NCs enclosed by {*hhl*} facets, concave HOH Au@Pd NCs enclosed by {*hkl*} facets, and THH Au@Pd NCs enclosed by {*hk*0} facets. The Miller indices of THH NCs could additionally be varied. These NCs with different crystallographic facets were electrocatalytically distinct in formic acid oxidation. This study shows that a seeded growth process combining the use of concave high-index TOH NC templates and kinetic control is a simple yet effective method for synthesizing noble metal NCs with adjustable high-index facets. This method of shape evolution reduces the efforts in kinetic tuning which would otherwise be needed if the high-index faceted NCs are to be formed without the templating NCs. It also improves the controllability of the surface structure of the NCs and offers new options in the shape-controlled synthesis of noble metal NCs.

Acknowledgment. We acknowledge the financial support from the Ministry of Education, Academic Research Grant R279-000-260-112. Y.Y. acknowledges the National University of Singapore for a research scholarship.

Supporting Information Available: Additional experimental details, additional TEM and FESEM images, elemental mapping by STEM-EDX, EDX spectra, and additional cyclic voltammograms. This material is available free of charge via the Internet at http://pubs.acs.org.

JA107405X